Report

Current Biology

Multiple Scales of Representation along the Hippocampal Anteroposterior Axis in Humans

Highlights

- Evidence of a coarse-to-fine representational scale along the hippocampal axis
- Voxel dynamics are more similar in anterior than posterior hippocampus
- More distinct dynamics relate to navigation and episodic simulation

Authors

Iva K. Brunec, Buddhika Bellana, Jason D. Ozubko, ..., Gordon Winocur, Morgan D. Barense, Morris Moscovitch

Correspondence

iva.kristlbrunec@mail.utoronto.ca (I.K.B.), b.bellana@mail.utoronto.ca (B.B.), barense@psych.utoronto.ca (M.D.B.), momos@psych.utoronto.ca (M.M.)

In Brief

Brunec, Bellana, et al. use fMRI to measure human hippocampal dynamics during virtual navigation and rest. Using two measures, higher similarity between voxels was found in the anterior, relative to the posterior hippocampus, consistent with rodent electrophysiology.

Brunec et al., 2018, Current Biology *28*, 2129–2135
July 9, 2018
https://doi.org/10.1016/j.cub.2018.05.016

CellPress

Current Biology
Report

Multiple Scales of Representation along the Hippocampal Anteroposterior Axis in Humans

Iva K. Brunec,[1,2,7,8,*] Buddhika Bellana,[1,2,7,*] Jason D. Ozubko,[3] Vincent Man,[1] Jessica Robin,[2] Zhong-Xu Liu,[2] Cheryl Grady,[1,2,6] R. Shayna Rosenbaum,[2,4] Gordon Winocur,[1,2,5,6] Morgan D. Barense,[1,2,*] and Morris Moscovitch[1,2,*]
[1]Department of Psychology, University of Toronto, Sidney Smith Hall, 100 St. George Street, Toronto, ON M5S 3G3, Canada
[2]Rotman Research Institute, Baycrest, Baycrest Centre for Geriatric Care, 3650 Baycrest Street, Toronto, ON M6A 2E1, Canada
[3]Department of Psychology, SUNY Geneseo, Bailey 133, 1 College Circle, Geneseo, NY 14454, USA
[4]Department of Psychology, York University, 4700 Keele Street, North York, ON M3J 1P3, Canada
[5]Department of Psychology, Trent University, Life and Health Sciences, DNA C104, Peterborough, ON K9J 7B8, Canada
[6]Department of Psychiatry, University of Toronto, 250 College Street, 8th Floor, Toronto, ON M5T 1R8, Canada
[7]These authors contributed equally
[8]Lead Contact
*Correspondence: iva.kristlbrunec@mail.utoronto.ca (I.K.B.), b.bellana@mail.utoronto.ca (B.B.), barense@psych.utoronto.ca (M.D.B.), momos@psych.utoronto.ca (M.M.)
https://doi.org/10.1016/j.cub.2018.05.016

SUMMARY

The ability to represent the world accurately relies on simultaneous coarse and fine-grained neural information coding, capturing both gist and detail of an experience. The longitudinal axis of the hippocampus may provide a gradient of representational granularity in spatial and episodic memory in rodents and humans [1–8]. Rodent place cells in the ventral hippocampus exhibit significantly larger place fields and greater autocorrelation than those in the dorsal hippocampus [1, 9–11], which may underlie a coarser and slower changing representation of space [10, 12]. Recent evidence suggests that properties of cellular dynamics in rodents can be captured with fMRI in humans during spatial navigation [13] and conceptual learning [14]. Similarly, mechanisms supporting granularity along the long axis may also be extrapolated to the scale of fMRI signal. Here, we provide the first evidence for separable scales of representation along the human hippocampal anteroposterior axis during navigation and rest by showing (1) greater similarity among voxel time courses and (2) higher temporal autocorrelation in anterior hippocampus (aHPC), relative to posterior hippocampus (pHPC), the human homologs of ventral and dorsal rodent hippocampus. aHPC voxels exhibited more similar activity at each time point and slower signal change over time than voxels in pHPC, consistent with place field organization in rodents. Importantly, similarity between voxels was related to navigational strategy and episodic memory. These findings provide evidence that the human hippocampus supports an anterior-to-posterior gradient of coarse-to-fine spatiotemporal representations, suggesting the existence of a cross-species mechanism, whereby lower neural similarity supports more complex coding of experience.

RESULTS AND DISCUSSION

If fMRI voxel-wise activation patterns are influenced by the increase in granularity stemming from larger place fields in anterior hippocampus (aHPC) (the homolog of ventral hippocampus in rodents) to smaller place fields in posterior hippocampus (pHPC) (dorsal in rodents), their fMRI time courses should be more similar to one another in aHPC, where the representations would be coarser (Figures 1A and 1B) than in pHPC. In addition, based on the reported increase in autocorrelation found in rodent place cell firing along the dorsoventral axis [9], voxel activation patterns may also show more autocorrelation over successive time points in aHPC than in pHPC (Figure 1B).

To test the hypothesis that dynamics of hippocampal activity in human fMRI reflect differences in representational scale along the hippocampal long axis, we calculated (1) correlations between voxel time courses within aHPC and pHPC (i.e., similarity in activity across voxels within an ROI; inter-voxel similarity, akin to [16]) and (2) stepwise autocorrelation of the fMRI signal for individual voxels within aHPC and pHPC (i.e., similarity in each voxel's activity across successive time points; temporal autocorrelation). We predicted that both types of neural similarity would be higher in aHPC compared to pHPC, corresponding to a coarser grain of representation and more slowly changing signal over time. We examined these measures during virtual reality navigation under different conditions of navigational difficulty to investigate, for the first time, neural dynamics underlying representational granularity along the hippocampal axis in humans (Figure 1C).

Participants in the navigation task (N = 19; see STAR Methods) traversed routes in a familiar virtualized environment (Toronto, Canada), using images from Google Street View (Figure 1C). Each participant traversed 16 routes while undergoing fMRI.

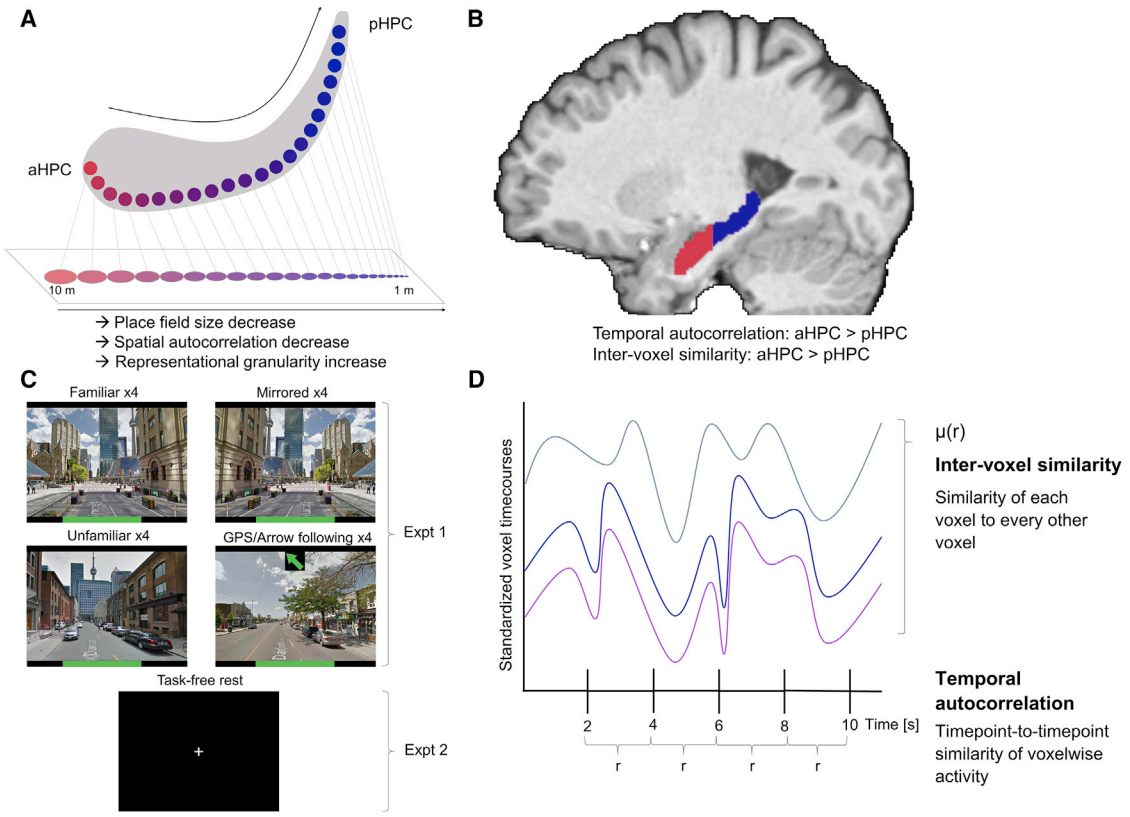

Figure 1. Overview of Experimental Methods and Analyses

(A) The hypothesized increase in representational scale along the anteroposterior axis is derived from rodent research suggesting a decrease from place field size in the ventral (anterior in humans) to dorsal (posterior in humans) hippocampus.

(B) Anterior (red) and posterior (blue) hippocampal masks, split at the uncal apex (see [15]), overlaid on an example brain in native space.

(C) In experiment 1, participants navigated in 4 conditions: familiar paths, unfamiliar paths, familiar paths where the environment was left-right reversed (mirrored), and unfamiliar paths where participants followed an arrow to navigate (GPS). The conditions scaled in navigational difficulty (GPS < familiar < unfamiliar < mirrored). In experiment 2, participants rested with their eyes closed and later reported how much time they spent engaging in episodic simulation (thinking about future episodes or remembering the past).

(D) Conceptualized data to illustrate inter-voxel similarity and temporal autocorrelation measures, where each line represents the time course of an individual voxel. Inter-voxel similarity was calculated as the mean of all unique time course correlations for each region, hemisphere, and condition per participant ($\mu(r)$). This is akin to measures of functional connectivity, calculated between voxels within a region of interest (ROI). Temporal autocorrelation was derived by calculating pairwise correlations for all voxels in an ROI across successive time points (TRs), stepwise, throughout an entire functional run. The mean of the resulting r-coefficients was calculated for each region, hemisphere, and condition per participant.

Bilateral hippocampal masks (defined using FreeSurfer) [17] were divided into anterior and posterior portions based on the location of the uncal apex for each participant, in their native space [2]. Using these masks, we then calculated (1) inter-voxel similarity and (2) temporal autocorrelation (Figure 1B).

To test for differences in inter-voxel similarity along the hippocampal axis, we conducted a 2 (axis: anterior and posterior) × 2 (hemisphere: left and right) × 4 (condition: familiar, unfamiliar, global positioning system [GPS], and mirrored; Figure 1C) repeated-measures ANOVA. Inter-voxel similarity was significantly greater in aHPC, relative to pHPC ($F(1, 18) = 49.17$; $p < 0.001$; Figure 2A), but there were no significant main effects of hemisphere ($F(1, 18) = 3.44$; $p = 0.08$) or condition ($F(3, 54) = 1.54$; $p = 0.214$). No interactions were significant (all p values ≥ 0.11).

To explore differences in temporal autocorrelation, an identical 2 (axis) × 2 (hemisphere) × 4 (condition) repeated-measures ANOVA was conducted. Like inter-voxel similarity, temporal autocorrelation was significantly greater in aHPC, relative to pHPC ($F(1, 18) = 15.51$; $p < 0.001$; Figure 2D). There was no main effect of hemisphere ($F(1, 18) = 0.683$; $p = 0.419$) and a trending interaction between axis and hemisphere ($F(1, 18) = 3.68$; $p = 0.071$; see Figure S4B). There was a significant main effect of condition ($F(3, 54) = 21.86$; $p < 0.001$), whereby autocorrelation scaled with increasing navigational difficulty. This effect as well as further effects of route-specific subjective difficulty are reported in Figure S2. No other interactions were significant (all p values > 0.19).

Critically, anteroposterior distinctions in hippocampal dynamics were related to navigational behavior. Participants' self-reported propensity to rely on map-based strategies in navigation was significantly negatively correlated with inter-voxel similarity in pHPC ($r = -0.526$; $p = 0.021$) and trended in the same direction in aHPC ($r = -0.403$; $p = 0.087$; Figure 2B,

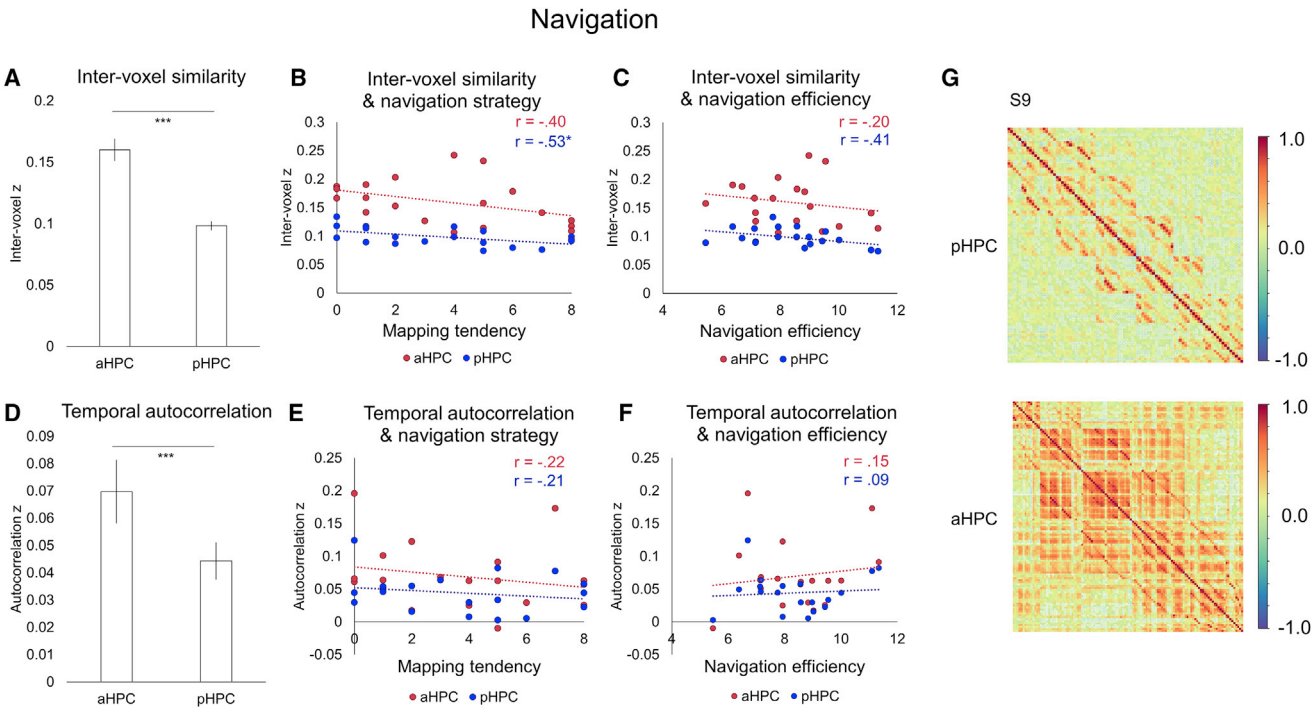

Figure 2. Hippocampal Long Axis Properties during Virtual Reality Navigation

(A) Inter-voxel similarity was significantly greater in aHPC, relative to pHPC, during navigation (r-coefficients were z-transformed before comparisons were made).

(B) Inter-voxel similarity in pHPC significantly negatively correlated with the tendency to use map-based navigation strategies (relative to landmark-based strategies).

(C) Inter-voxel similarity in pHPC, but not aHPC, negatively correlated with in-scan navigational efficiency.

(D) Autocorrelation was significantly greater in aHPC, relative to pHPC during navigation.

(E) No significant relationships between temporal autocorrelation and navigation tendency were found.

(F) Unlike inter-voxel similarity, autocorrelation showed no relationship with in-scan navigational efficiency. For further analyses, please refer to Figure S2.

(G) Inter-voxel correlation matrices for a sample participant (aHPC and pHPC in the left hemisphere; collapsed across navigation conditions because no significant main effect of condition was found). Voxels in aHPC were consistently more correlated with one another than voxels in pHPC within each participant. For individual matrices for all participants, see Figure S1.

***$p < 0.001$; *$p < 0.05$. All error bars are SEM. See also Figure S4 and Tables S2 and S3.

full questionnaire in STAR Methods). Lower similarity among hippocampal voxels may imply finer-grained coding, as the signal is less redundant and can contain more complex information. Reduced similarity may relate to a greater propensity to use more complex, map-based navigational strategies that rely on discrimination between fine-grained spatial representations [18]. To support this notion, we also found a negative trend in the correlation between pHPC inter-voxel similarity and navigational efficiency in the navigation task ($r = -0.413$; $p = 0.079$), where more efficient navigators had lower inter-voxel similarity in pHPC. No such relationship was observed in aHPC ($r = 0.199$; $p = 0.414$; Figure 2C). Navigational efficiency was calculated as the average decrease in Euclidean distance to the goal between steps (greater difference therefore indicates greater navigational efficiency). Correspondingly, there was a significant relationship between self-reported mapping propensity and navigational efficiency ($r = 0.560$; $p = 0.013$), indicating that participants with greater mapping propensity navigated more efficiently toward the goal.

There was no significant relationship between map-based navigation and temporal autocorrelation in pHPC ($r = -0.207$; $p = 0.394$) and no significant relationship with aHPC ($r = -0.217$; $p = 0.372$; Figure 2E). There was no significant relationship between navigational efficiency and temporal autocorrelation in aHPC ($r = 0.146$; $p = 0.550$) or pHPC ($r = 0.086$; $p = 0.726$; Figure 2F).

Inter-voxel similarity and temporal autocorrelation were not significantly correlated in aHPC ($r = 0.217$; $p = 0.372$) or pHPC ($r = -0.133$; $p = 0.589$), suggesting that they capture separable aspects of hippocampal coding. Inter-voxel similarity values in aHPC and pHPC were not significantly correlated ($r = 0.295$; $p = 0.220$), but autocorrelation varied consistently along the hippocampal axis ($r = 0.879$; $p < 0.001$).

To establish whether these findings were task driven (i.e., navigation dependent) or whether they reflect a task-independent property of hippocampal dynamics, we examined the same measures in a resting state dataset carried out on a separate group of 20 participants [19]. Resting state has no explicit demand on behavior, although continuous dynamics can still be measured, making it an ideal contrast to navigation. If the observed distinction in anteroposterior hippocampal signal dynamics extends from navigation to rest, it would provide clear evidence that this anteroposterior distinction is not dependent on navigation. To this effect, we conducted 2 (axis) × 2

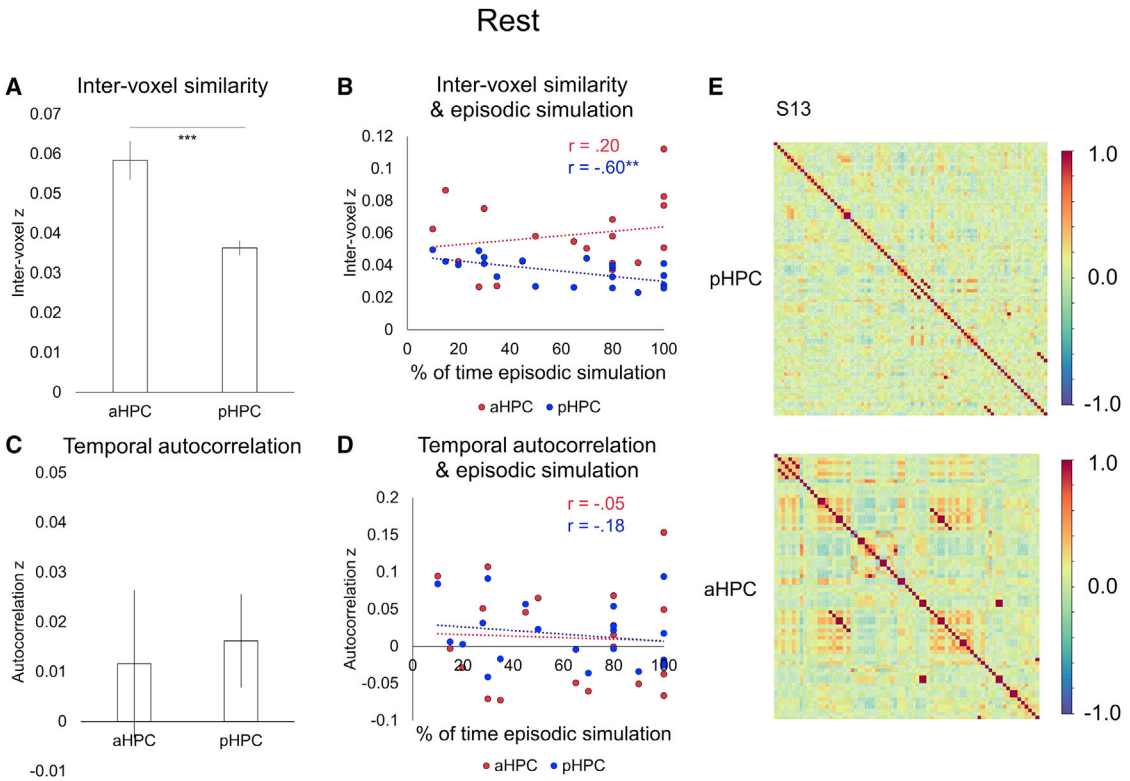

Figure 3. Hippocampal Long Axis Properties during Task-free Rest

(A) Inter-voxel similarity was significantly greater in aHPC, relative to pHPC during rest.

(B) Inter-voxel similarity in pHPC significantly negatively correlated with self-reported time spent in episodic simulation (i.e., thinking about the past or simulating the future).

(C) Autocorrelation was not significantly different between aHPC and pHPC at rest.

(D) No significant relationships between temporal autocorrelation and episodic simulation were found. For further analyses, please refer to Figures S2 and S3.

(E) Inter-voxel correlation matrices for a sample participant (aHPC and pHPC in the left hemisphere). Voxels in aHPC were consistently more correlated with one another than voxels in pHPC within each participant. For individual matrices for all participants, see Figure S1.

***$p < 0.001$; *$p < 0.05$. All error bars are SEM. See also Figure S4 and Tables S2 and S3.

(hemisphere) repeated-measures ANOVAs on both inter-voxel similarity and temporal autocorrelation, using participant-specific aHPC and pHPC masks generated in native space using an identical procedure to the previous navigation analysis.

As in navigation, resting inter-voxel similarity was significantly greater in aHPC, relative to pHPC ($F(1, 19) = 17.04$; $p < 0.001$; Figure 3A). There was no significant effect of hemisphere ($F(1, 19) = 0.528$; $p = 0.476$) and no significant axis by hemisphere interaction ($F(1, 19) = 0.100$; $p = 0.755$).

In contrast to navigation, there was no significant difference in resting temporal autocorrelation between aHPC and pHPC ($F(1, 19) = 0.418$; $p = 0.526$; Figure 3C), nor was there a significant main effect of hemisphere ($F(1, 19) = 0.646$; $p = 0.431$) or axis by hemisphere interaction ($F(1, 19) = 1.34$; $p = 0.261$). The absence of a continuous external context during rest, unlike during navigation, may underlie the lack of temporal autocorrelation effects in the hippocampus (for more detailed lag analyses, see Figure S2).

These data suggest that the observed distinction in hippocampal signal dynamics along the anteroposterior axis is not entirely navigation dependent, where some of these properties may be fundamental to aHPC and pHPC across task and resting state. However, as the anteroposterior distinction was most robust during navigation, it appears to be modulated by ongoing task demands.

Although resting state scans involve no explicit processing demands, the degree to which participants engage in typically hippocampus-dependent thought, such as thinking about the past or the future, may vary [19]. Participants' self-reported in-scan episodic simulation (i.e., the percentage of the resting scan where they were either remembering past or imagining future episodes) was significantly negatively correlated with inter-voxel similarity in pHPC ($r = -0.606$; $p = 0.005$), but not aHPC ($r = 0.200$; $p = 0.399$), akin to the relation found for map-based strategies in the navigation data (Figure 3B). More variability in neural signal during episodic simulation may reflect more dynamic content or increased episodic detail. There was no significant relationship between temporal autocorrelation and self-reported episodic simulation in either aHPC ($r = -0.049$; $p = 0.837$) or pHPC ($r = -0.183$; $p = 0.441$; Figure 3D).

Inter-voxel similarity and temporal autocorrelation were again not significantly correlated with one another in aHPC ($r = 0.026$; $p = 0.913$) or pHPC ($r = 0.171$; $p = 0.470$) at rest. As in navigation, there was no significant correlation between inter-voxel similarity

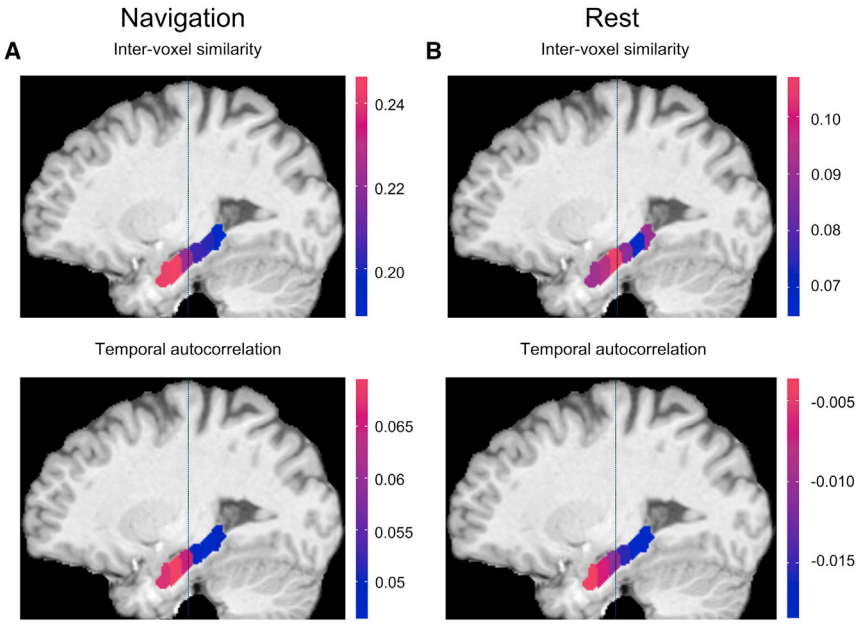

Figure 4. Representational Gradients along the Anteroposterior Axis

Mean inter-voxel similarity and temporal autocorrelation model fits, corrected for distance between voxels (see Figure S3) within each segment, plotted according to their magnitude along the hippocampal long axis in (A) navigation and (B) resting state. See also Figure S2 and Table S1.

values in aHPC and pHPC ($r = -0.087$; $p = 0.715$) but a significant relationship between temporal autocorrelation in aHPC and pHPC ($r = 0.926$; $p < 0.001$).

To visualize differences in inter-voxel similarity along the hippocampal axis with finer spatial resolution, bilateral hippocampal masks were split into 6 segments with inter-voxel similarity calculated for each segment separately (Figure 4A). Inter-voxel similarity was again generally higher in segments anterior to the uncal apex relative to posterior segments, supporting the initial dichotomy (for details, see Supplemental Information; Figure S3). Temporal autocorrelation appeared to have a smooth linear gradient with the highest autocorrelation in the head of the aHPC and least in the most posterior segments of the pHPC (Figure 4; for details, see Supplemental Information; Figure S3).

A series of control analyses were conducted to ensure that the observed anteroposterior differences in signal similarity were not due to differences in hippocampal shape along the longitudinal axis or overall differences in temporal or spatial signal-to-noise ratio (SNR) between the aHPC and pHPC. Results indicated that the differences between aHPC and pHPC in inter-voxel similarity and temporal autocorrelation could not be explained by hippocampal shape or spatial or temporal SNR alone (for details, see Figure S3 and Tables S1, S2, and S3). In both datasets, temporal and spatial SNR were higher in pHPC, but when SNR was added to our model, the main effect of axis on inter-voxel similarity and temporal autocorrelation remained unchanged (Tables S2 and S3). Additional control analyses further determined that the coarse-to-fine distinction along the anteroposterior axis was unique to the hippocampus and not present in the neighboring parahippocampal cortex (for details, see Figure S4). In combination, these control analyses provide strong support for a distinct pattern of spatiotemporal dynamics between the anterior and posterior hippocampus in humans.

Using two measures to investigate human hippocampal activity during navigation and rest, we show evidence for a robust distinction between anterior and posterior hippocampal dynamics. Neural dynamics in pHPC were not only more variable at each moment in time (inter-voxel similarity) but also shifted more rapidly between successive time points (temporal autocorrelation), relative to aHPC during navigation. Overall levels of temporal autocorrelation were found to scale with navigational difficulty, but the difference between aHPC and pHPC remained stable. This suggests that greater navigational effort enhances the degree to which unfolding spatiotemporal context must be maintained but does not differentially modulate signal in aHPC and pHPC. In contrast, inter-voxel similarity differences in aHPC and pHPC were not affected by navigational condition, suggesting that signal complexity within these brain regions is robust to fluctuations in task demands. However, although the difference in inter-voxel similarity between aHPC and pHPC remained significant during rest, the overall level of inter-voxel similarity was significantly lower than during navigation (Figure S4). The latter finding suggests that, when there is no goal direction, as is the case in rest, neural activity is relatively uncoordinated compared to activity in structured navigational tasks. No significant difference was found in temporal autocorrelation between aHPC and pHPC (though see Figures S2 and S3). This pattern was unique to the hippocampus and not observed in the parahippocampal cortex, a region in close anatomical proximity to the hippocampus and strongly functionally connected with it [20], suggesting the anteroposterior difference in neural dynamics reported here is a fundamental and distinctive organizing property of the hippocampus. Although this control analysis suggests that the same signal properties are not present across the entire medial temporal lobes (MTLs), precise characterization of signal properties in cortical and subcortical inputs to the hippocampus is necessary in future investigations, ideally in combination with fine-grained functional connectivity analyses.

The difference in spatiotemporal representational granularity along the hippocampal axis may therefore rely on underlying neural dynamics, which in aHPC, relative to pHPC, produce (1) greater similarity between individual voxel time courses and (2) slower changes in activity. These results also suggest that the cellular mechanisms observed in rodents [9, 10] may have effects that scale up to the timescales of fMRI, underlying the reported findings of increased representational granularity along the axis in memory [15], narratives [3, 4], and spatial navigation [6, 21]. Greater neural similarity in aHPC supports the notion that voxels remain in the same state for longer periods of time

than in pHPC, which may enable effective representation of slow-changing global context signals, such as the gist of an episode or a large spatial context. Our results generally provide evidence for a coarse-to-fine gradient along the hippocampal long axis. Temporal autocorrelation showed a clear linear decrease in similarity from aHPC to pHPC in both navigation and resting state, but inter-voxel similarity only showed a linear trend in navigation once we accounted for differences in hippocampal shape (Figure S3). Further treatment of this issue with higher resolution imaging of the hippocampus is warranted to better understand the organization of the hippocampal long axis.

Critically, differences in signal dynamics between aHPC and pHPC were also reflected in behavior across both navigation and resting datasets. Greater propensity for map-based navigation strategies was related to lower hippocampal inter-voxel similarity. Greater propensity for map-based navigation strategies was related to lower hippocampal inter-voxel similarity. Lower similarity may suggest representation of more complex information content, consistent with the use of cognitive maps [18], though this relationship warrants empirical examination. Lower inter-voxel similarity in pHPC signal also corresponded to increased self-reported episodic memory processing during rest. Remembering past and imagining future episodes reliably recruits regions of the MTL [19, 22], and greater dissimilarity among hippocampal voxels may reflect increased elaboration in episodic memory [15] and simulation [23].

At a more general level, our findings suggest that differences in the intrinsic dynamics of hippocampal neurons may underlie or support the cognitive functions mediated by them, such as aspects of spatial navigation and episodic memory. Differences in whole-brain and intra-hippocampal functional connectivity between aHPC and pHPC may also contribute to specialization along the long axis of the hippocampus [20, 24, 25]. Robust differences in representational scale between aHPC and pHPC were found despite the fact that our measures did not directly manipulate demands on granularity per se. Future studies are needed to determine whether changes in the representational demands of the task will be reflected in changes in signal granularity as assessed by inter-voxel similarity and temporal autocorrelation or whether changes in task demands will merely determine where along the axis activation is most pronounced.

The novel evidence presented here supports a cross-species generalization of hippocampal function, revealing a potential fundamental principle by which the hippocampus codes temporally extended experiences. Applying the approach to processing dynamics of hippocampus reported in this study to any temporally extended fMRI dataset opens new doors for exploring potential differential trajectories in aging and disease and individual differences in normal memory and cognition.

STAR★METHODS

Detailed methods are provided in the online version of this paper and include the following:

SUPPLEMENTAL INFORMATION

Supplemental Information includes four figures and three tables and can be found with this article online at https://doi.org/10.1016/j.cub.2018.05.016.

ACKNOWLEDGMENTS

This work was supported by Canadian Institute of Health Research grants (no. 49566 and no. 125958) to R.S.R., C.G., G.W., and M.M. I.K.B. is supported by an Alzheimer Society Canada doctoral award (no. 17-19).

AUTHOR CONTRIBUTIONS

I.K.B., B.B., M.D.B., and M.M. generated the hypotheses; I.K.B. and B.B. developed the analytic approach, planned, and carried out the analyses, with input from J.D.O., J.R., V.M., Z.-X.L., C.G., R.S.R., G.W., M.D.B., and M.M. The navigation paradigm was designed by J.D.O., J.R., C.G., R.S.R., G.W., and M.M. and implemented by J.D.O. J.D.O., J.R., and Z.-X.L. collected the data. J.R. developed the navigational strategies questionnaire. All authors contributed to writing the manuscript and approved of the final version of the submitted manuscript.

DECLARATION OF INTERESTS

The authors declare no competing interests.

Received: October 21, 2017
Revised: February 21, 2018
Accepted: May 8, 2018
Published: June 21, 2018

REFERENCES

1. Strange, B.A., Witter, M.P., Lein, E.S., and Moser, E.I. (2014). Functional organization of the hippocampal longitudinal axis. Nat. Rev. Neurosci. *15*, 655–669.
2. Poppenk, J., Evensmoen, H.R., Moscovitch, M., and Nadel, L. (2013). Long-axis specialization of the human hippocampus. Trends Cogn. Sci. *17*, 230–240.
3. Collin, S.H.P., Milivojevic, B., and Doeller, C.F. (2015). Memory hierarchies map onto the hippocampal long axis in humans. Nat. Neurosci. *18*, 1562–1564.
4. Milivojevic, B., and Doeller, C.F. (2013). Mnemonic networks in the hippocampal formation: from spatial maps to temporal and conceptual codes. J. Exp. Psychol. Gen. *142*, 1231–1241.

5. Robin, J., and Moscovitch, M. (2017). Details, gist and schema: hippocampal–neocortical interactions underlying recent and remote episodic and spatial memory. Curr. Opin. Behav. Sci. *17*, 114–123.
6. Evensmoen, H.R., Lehn, H., Xu, J., Witter, M.P., Nadel, L., and Håberg, A.K. (2013). The anterior hippocampus supports a coarse, global environmental representation and the posterior hippocampus supports fine-grained, local environmental representations. J. Cogn. Neurosci. *25*, 1908–1925.
7. Nadel, L., Hoscheidt, S., and Ryan, L.R. (2013). Spatial cognition and the hippocampus: the anterior-posterior axis. J. Cogn. Neurosci. *25*, 22–28.
8. Morton, N.W., Sherrill, K.R., and Preston, A.R. (2017). Memory integration constructs maps of space, time, and concepts. Curr. Opin. Behav. Sci. *17*, 161–168.
9. Kjelstrup, K.B., Solstad, T., Brun, V.H., Hafting, T., Leutgeb, S., Witter, M.P., Moser, E.I., and Moser, M.B. (2008). Finite scale of spatial representation in the hippocampus. Science *321*, 140–143.
10. Maurer, A.P., Vanrhoads, S.R., Sutherland, G.R., Lipa, P., and McNaughton, B.L. (2005). Self-motion and the origin of differential spatial scaling along the septo-temporal axis of the hippocampus. Hippocampus *15*, 841–852.
11. Keinath, A.T., Wang, M.E., Wann, E.G., Yuan, R.K., Dudman, J.T., and Muzzio, I.A. (2014). Precise spatial coding is preserved along the longitudinal hippocampal axis. Hippocampus *24*, 1533–1548.
12. Brun, V.H., Solstad, T., Kjelstrup, K.B., Fyhn, M., Witter, M.P., Moser, E.I., and Moser, M.-B. (2008). Progressive increase in grid scale from dorsal to ventral medial entorhinal cortex. Hippocampus *18*, 1200–1212.
13. Doeller, C.F., Barry, C., and Burgess, N. (2010). Evidence for grid cells in a human memory network. Nature *463*, 657–661.
14. Constantinescu, A.O., O'Reilly, J.X., and Behrens, T.E.J. (2016). Organizing conceptual knowledge in humans with a gridlike code. Science *352*, 1464–1468.
15. Poppenk, J., and Moscovitch, M. (2011). A hippocampal marker of recollection memory ability among healthy young adults: contributions of posterior and anterior segments. Neuron *72*, 931–937.
16. Tambini, A., and Davachi, L. (2013). Persistence of hippocampal multivoxel patterns into postencoding rest is related to memory. Proc. Natl. Acad. Sci. USA *110*, 19591–19596.
17. Fischl, B. (2012). FreeSurfer. Neuroimage *62*, 774–781.
18. Maguire, E.A., Gadian, D.G., Johnsrude, I.S., Good, C.D., Ashburner, J., Frackowiak, R.S.J., and Frith, C.D. (2000). Navigation-related structural change in the hippocampi of taxi drivers. Proc. Natl. Acad. Sci. USA *97*, 4398–4403.
19. Bellana, B., Liu, Z.X., Diamond, N.B., Grady, C.L., and Moscovitch, M. (2017). Similarities and differences in the default mode network across rest, retrieval, and future imagining. Hum. Brain Mapp. *38*, 1155–1171.
20. Libby, L.A., Ekstrom, A.D., Ragland, J.D., and Ranganath, C. (2012). Differential connectivity of perirhinal and parahippocampal cortices within human hippocampal subregions revealed by high-resolution functional imaging. J. Neurosci. *32*, 6550–6560.
21. Howard, L.R., Javadi, A.H., Yu, Y., Mill, R.D., Morrison, L.C., Knight, R., Loftus, M.M., Staskute, L., and Spiers, H.J. (2014). The hippocampus and entorhinal cortex encode the path and Euclidean distances to goals during navigation. Curr. Biol. *24*, 1331–1340.
22. Addis, D.R., and Schacter, D.L. (2008). Constructive episodic simulation: temporal distance and detail of past and future events modulate hippocampal engagement. Hippocampus *18*, 227–237.
23. Addis, D.R., and Schacter, D.L. (2012). The hippocampus and imagining the future: where do we stand? Front. Hum. Neurosci. *5*, 173.
24. Buzsáki, G., and Moser, E.I. (2013). Memory, navigation and theta rhythm in the hippocampal-entorhinal system. Nat. Neurosci. *16*, 130–138.
25. Zeidman, P., and Maguire, E.A. (2016). Anterior hippocampus: the anatomy of perception, imagination and episodic memory. Nat. Rev. Neurosci. *17*, 173–182.
26. MathWorks (2012). MATLAB and statistics toolbox release (The MathWorks). https://www.mathworks.com/.
27. Penny, W.D., Friston, K.J., Ashburner, J.T., Kiebel, S.J., and Nichols, T.E., eds. (2011). Statistical Parametric Mapping: The Analysis of Functional Brain Images (Academic).
28. Smith, S.M., Jenkinson, M., Woolrich, M.W., Beckmann, C.F., Behrens, T.E., Johansen-Berg, H., Bannister, P.R., De Luca, M., Drobnjak, I., Flitney, D.E., et al. (2004). Advances in functional and structural MR image analysis and implementation as FSL. Neuroimage *23* (*Suppl 1*), S208–S219.
29. Cox, R.W. (1996). AFNI: software for analysis and visualization of functional magnetic resonance neuroimages. Comput. Biomed. Res. *29*, 162–173.
30. R Development Core Team (2008). R: a language and environment for statistical computing (R Foundation for Statistical Computing). http://www.R-project.org.
31. RStudio Team (2016). RStudio: integrated development for R (RStudio). http://www.rstudio.com/.
32. Martin, A.D., Quinn, K.M., and Park, J.H. (2011). MCMCpack: Markov Chain Monte Carlo in R. J. Stat. Softw. *42*, 1–21.
33. Wei, T., Simko, V., Levy, M., Xie, Y., Jin, Y., and Zemla, J. (2016). corrplot: visualization of a correlation matrix. R package version 0.77. http://CRAN.R-project.org/package=corrplot.
34. Psychology Software Tools (2012). E-Prime 2.0. http://www.pstnet.com.
35. Brainard, D.H. (1997). The psychophysics toolbox. Spat. Vis. *10*, 433–436.
36. Pinheiro, J., Bates, D., DebRoy, S., Sarkar, D., Heisterkamp, S., and Van Willigen, B.; R Core Team (2017). nlme: linear and nonlinear mixed effects models. R package version 3.1-131. https://CRAN.R-project.org/package=nlme.
37. Hegarty, M., Richardson, A.E., Montello, D.R., Lovelace, K., and Subbiah, I. (2002). Development of a self-report measure of environmental spatial ability. Intelligence *30*, 425–447.
38. Power, J.D., Barnes, K.A., Snyder, A.Z., Schlaggar, B.L., and Petersen, S.E. (2012). Spurious but systematic correlations in functional connectivity MRI networks arise from subject motion. Neuroimage *59*, 2142–2154.
39. Campbell, K.L., Grigg, O., Saverino, C., Churchill, N., and Grady, C.L. (2013). Age differences in the intrinsic functional connectivity of default network subsystems. Front. Aging Neurosci. *5*, 73.
40. Aguirre, G.K., Detre, J.A., Alsop, D.C., and D'Esposito, M. (1996). The parahippocampus subserves topographical learning in man. Cereb. Cortex *6*, 823–829.
41. Janzen, G., and van Turennout, M. (2004). Selective neural representation of objects relevant for navigation. Nat. Neurosci. *7*, 673–677.

STAR★METHODS

KEY RESOURCES TABLE

REAGENT or RESOURCE	SOURCE	IDENTIFIER
Software and Algorithms		
Inter-voxel Similarity & Temporal Autocorrelation Code	Custom software	https://github.com/ivabrunec/Voxel_Temporal_Patterns
MATLAB 2014b	MathWorks [26]	https://www.mathworks.com
SPM	Wellcome Department of Cognitive Neurology, London, UK [27]	http://www.fil.ion.ucl.ac.uk/spm/
FSL 5.0.9	FMRIB Software Library [28]	https://fsl.fmrib.ox.ac.uk/fsl/fslwiki/
AFNI	[29]	https://afni.nimh.nih.gov/
R version 3.4.2, RStudio interface	[30, 31]	https://www.r-project.org/
MCMCPack	[32]	http://www.jstatsoft.org/v42/i09/
Corrplot	[33]	http://CRAN.R-project.org/package=corrplot
E-Prime	[34]	http://www.pstnet.com
Psychophysics Toolbox	[35]	http://psychtoolbox.org/
nlme	[36]	https://cran.r-project.org/web/packages/nlme/

CONTACT FOR REAGENT AND RESOURCE SHARING

Further information and requests for resources and reagents should be directed to and will be fulfilled by the Lead Contact, Iva Brunec (iva.kristlbrunec@mail.utoronto.ca).

EXPERIMENTAL MODEL AND SUBJECT DETAILS

Experiment 1: Virtual Route Navigation

Subjects

Twenty-two healthy right-handed volunteers were recruited. One participant was excluded because of excessive difficulty with the task (i.e., repeatedly getting lost). Two additional participants were excluded due to incomplete data or technical issues. Exclusions resulted in 19 participants who completed the study (9 males; mean age 22.58 years, range 19-30 years). All participants had lived in Toronto for at least 2 years ($M = 10.45$, $SE = 1.81$). All participants were free of psychiatric and neurological conditions. All participants had normal or corrected-to-normal vision and otherwise met the criteria for participation in fMRI studies. Informed consent was obtained from all participants in accordance with Rotman Research Institute at Baycrest's ethical guidelines. Participants received monetary compensation upon completion of the study.

Experiment 2: Resting State

Subjects

A separate set of twenty healthy right-handed volunteers were recruited. All participants who were recruited completed the study (9 males; mean age 22.58 years, range 19-30 years). A 6-minute resting state scan was collected per participant at the beginning of a longer memory experiment (see [19]). All were native English speakers, and free of any psychiatric or neurological conditions. Informed consent was obtained from all participants in accordance with the Rotman Research Institute at Baycrest's ethical guidelines. Participants received monetary compensation upon completion of the study.

METHOD DETAILS

Experiment 1: Virtual Route Navigation Procedure

City Virtualization Materials

A custom software suite was designed to access the first-person images from Google Street View, which was used to download an approximately 42 × 27 km region of Toronto, Canada. Images were used to reconstruct a photorealistic, virtual simulation of Toronto (see Navigation Task below).

Prescan Route Building

There were four conditions, based on increasing navigational difficulty: GPS, Familiar, Unfamiliar, and Mirrored. The routes were constructed prior to the date of scanning: participants built routes with researcher assistance, using a computer program which showed overhead maps of Toronto. Participants defined 8 routes with which they were highly familiar, and 4 routes with which they were less familiar. Because participants varied in their familiarity with Toronto, high and low familiarity routes for each participant were not uniform, and hence these routes varied in terms of geography and design from participant to participant. For low familiarity routes (Unfamiliar condition), participants were asked to choose two places or landmarks in Toronto with which they were familiar, but between which they had never directly traveled. For the highly familiar routes (Familiar condition), participants were asked to produce their most familiar routes between their personally common destinations in Toronto (e.g., home to school, home to work, etc.). Without input from participants, 4 of the 8 highly familiar routes were selected by the researcher to be mirrored. The motivation for the Mirrored condition was to gain insight into hippocampal processing under high navigational difficulty, such as when reconfiguring familiar routes. Participants thus had to rely on their hippocampal representations and consider the relations between landmarks. The mirror manipulation involved flipping the visual image on the computer screen left-to-right, thus functionally flipping participants' navigational decisions. Additionally, a set of 4 routes in areas of Toronto with which the participant reported no previous experience was created by the researcher to be used in the baseline (GPS) condition.

These conditions were thus designed to modulate task demands by increasing navigational difficulty.

Prescan Interview

On the day of the experiment, participants first completed a prescan interview and practice session. The interview included a survey to assess participants' propensity and ability to use maps for navigation and the Santa Barbara Sense of Direction Scale (SBSOD) [37], to obtain a measure of navigational ability. This was followed by a detailed description of the navigation task along with practice trials with routes not used in scanning. There was no significant correlation between SBSODS scores and inter-voxel similarity in aHPC ($r = 0.214$, $p = 0.379$) or pHPC ($r = -.266$, $p = 0.272$). There was a trending correlation between SBSODS scores and temporal autocorrelation in aHPC ($r = 0.451$, $p = 0.053$) and no significant correlation in pHPC ($r = 0.292$, $p = 0.225$).

Navigational Strategies Questionnaire

The navigational strategies questionnaire, used to assess propensity for map-based navigation, is reproduced here:

Note: Each response had an answer corresponding to a map-based navigation strategy or characteristic (indicated in bold) and one corresponding to a non-map/scene-based strategy (underlined). The mapping tendency was calculated as the difference between the number of map-based answers and non-map-based answers. Some questions had a third alternative, which was not coded.

This questionnaire contains questions about your experience navigating, the strategies you use, and what helps you to navigate. Circle the answer for each question that best describes how you navigate, or describe your answer in the space beside "Other" if neither applies.

1. When planning a route, do you picture a map of your route or do you picture scenes of what you will see along the way?

Map Scenes Other: _____

2. Do you consider yourself a good navigator?

Yes No

3. Do you find it easy to read and use maps?

Yes Somewhat No

4. How often do you get disoriented while finding your way around?

Very often Somewhat often **Very rarely**

5. When thinking about a familiar street, how well can you picture the buildings along it?

Very clearly Somewhat clearly **Hardly at all**

6. Would you give directions to a friend in terms of landmarks (i.e., when you see the subway stop, turn left?) or in terms of map directions (i.e., walk north four blocks, then turn left?)?

Landmarks **Map Directions** Other: _____

7. Do you picture traveling a route on street level or from a bird's eye view?

Street-level **Bird's Eye View** Other: _____

8. When navigating in an area you know well, do you usually just know where to go or do you need to look around at the surroundings to decide (e.g., coming out of a subway station)?

Know it Some of each Need to look around

9. When traveling along a new route, do you usually remember what buildings you've passed?

Yes Somewhat **Rarely**

10. Would you prefer to navigate using a list of directions or a map?

Directions **Map** No preference

11. Do you use landmarks (i.e., familiar buildings) to orient yourself when navigating?

Often Sometimes **Rarely**

12. Do you find you're flexible navigating along routes (i.e., you can take new shortcuts easily), or do you prefer to follow the same path every time?

Flexible Somewhat flexible Prefer the same route
13. How easily could you draw a map of an area of the city that you know well?
Very easily Somewhat easily Not easily
14. Do you think that you navigate by following a mental map, or working on scene at a time?
Maps Scene at a time Other

Navigation Task

The navigation software was written in MATLAB v7.5.0.342 and used the PsychToolbox v3.0.10 [26, 35]. The software used first-person images from Google Street View to allow participants to walk through a virtual Toronto. Navigation was controlled using three buttons: left, right, and forward. A "done" button allowed participants to indicate that they had completed a route. The task was projected on a screen in the bore of the scanner viewed by the participants through a mirror mounted inside of the head coil.

Participants navigated 16 routes: 4 Familiar, 4 Unfamiliar, 4 Mirrored, and 4 GPS baseline routes. The order of routes was randomized for each participant. On each route, except GPS routes, participants were given a destination and had to navigate toward that destination. Participants navigated from a first-person, street-level perspective. GPS trials involved no goal-directed navigation; instead, participants followed a dynamic arrow (see Figure 1C).

Every route contained 3-4 turns and was 2-10 km long. The average run (route) length was 137.6 TRs (2 s TRs). The average number of TRs was lowest in the GPS condition (M = 92.13, SD = 17.44), followed by the familiar condition (M = 136.45, SD = 39.18), the mirrored condition (M = 155.73, SD = 36.84), and the unfamiliar condition (M = 158.78, SD = 32.13). An analysis controlling for route length is reported in Supplemental Information (see legend for Figure S2A). We ran a linear mixed effects model examining autocorrelation and inter-voxel similarity on each run. We extracted the number of TRs for each route, performed a median split and used length (short versus long runs) as a categorical predictor, along with axis (aHPC versus pHPC), hemisphere (L versus R), and condition (GPS, Familiar, Unfamiliar, Mirrored), with subjects as a random factor.

The average navigational efficiency differed between conditions, such that participants navigated most efficiently (greatest decrease in Euclidean distance to goal per step) during route following (GPS) (M = 11.04, SD = 1.56), followed by familiar routes (M = 10.45, SD = 2.06), unfamiliar routes (M = 7.90, SD = 2.54), and were least efficient at navigating mirrored routes (M = 4.97, SD = 2.84). Navigational efficiency therefore decreased as the condition-level navigational difficulty increased.

After completing each route, participants provided two behavioral ratings. They rated how familiar each route felt, and how difficult they found it to navigate on a scale from 1-9 (where 1 would correspond to least familiar and most difficult, respectively). For example, two routes might have different levels of familiarity despite both being in the Familiar condition. As expected, the average reported familiarity scaled as expected: 1) Familiar condition (M = 7.0, SD = 1.79), 2) Mirrored condition (M = 5.36, SD = 2.69), 3) Unfamiliar condition (M = 4.35, SD = 2.38), 4) GPS condition (M = 3.0, SD = 1.06). Self-reported familiarity ratings of individual routes therefore corresponded to the experimental manipulation. The GPS condition was, however, rated as the easiest (M = 7.2, SD = 1.46), followed by the Familiar condition (M = 6.98, SD = 2.05), Unfamiliar condition (M = 4.35, SD = 2.66), and the Mirrored condition, which was subjectively the most difficult (M = 3.97, SD = 2.42).

These ratings suggest that the four conditions differed in terms of their navigational difficulty, such that GPS routes were subjectively least demanding to navigate, and Mirrored routes were most demanding. An analysis of temporal autocorrelation split by route-specific subjective difficulty is reported in Supplemental Information (Figure S2). We performed a median split of difficulty ratings within each condition. To investigate subjective difficulty on each route, we entered the rating category resulting from the median split (easy versus difficult) for each route as a predictor in a linear mixed effects model, along with axis, hemisphere, and condition as predictors, and subjects as a random factor. We chose not to explore familiarity ratings, as they were collected to confirm the condition manipulation (GPS routes least, Familiar routes most familiar; there were almost no familiar GPS routes).

fMRI Image Acquisition

Participants were scanned with a 3T Siemens MRI scanner at Baycrest's Rotman Research Institute. A high-resolution 3D MPRAGE T1-weighted pulse sequence image (160 axial slices, 1 mm thick, FOV = 256 mm) was first obtained to register functional maps against brain anatomy. Functional imaging was performed to measure brain activation by means of the blood oxygenation level-dependent (BOLD) effect. Functional T2*-weighted images were acquired using echo-planar imagine (30 axial slices, 5 mm thick, TR = 2000 ms, TE = 30 ms, flip angle = 70 degrees, FOV = 200 mm). The native EPI resolution was 64 × 64 with a voxel size of 3.5mm x 3.5mm x 5.0mm. Images were first corrected for physiological motion using the Analysis of Functional NeuroImages [29]. All subsequent analysis steps were conducted using the statistical parametric mapping software SPM12 [27]. Preprocessing involved slice timing correction, spatial realignment and co-registration, with a resampled voxel size of 3 mm isotropic, with no spatial smoothing. As all of our analyses rely on covariance, we additionally regressed out the mean time-courses from participant-specific white matter, and cerebrospinal fluid masks, alongside estimates of the 6 rigid body motion parameters from each EPI run. To further correct for the effects of motion which may persist despite standard processing [38], an additional motion scrubbing procedure was added to the end of our preprocessing pipeline [39]. Using a conservative multivariate technique, time points that were outliers in both the six rigid-body motion parameter estimates and BOLD signal were removed, and outlying BOLD signal was replaced by interpolating across neighboring data points. Motion scrubbing further minimizes any effects of motion-induced spikes on the BOLD signal, over and beyond standard motion regression, without leaving sharp discontinuities due to the removal of outlier volumes (for details, see [39]).

Experiment 2: Resting State Procedure

After an anatomical MRI scan, participants first completed a standard 6-minute resting scan (180 2 s TRs) in which they were asked to keep their eyes closed and remain still, relaxed, and awake. They were also allowed to think freely, without any explicit constraints (for additional details, see [19]). E- Prime software (v2, [34]) was used to present the instructions for the functional runs, projected on a screen in the bore of the scanner viewed by the participants through a mirror mounted inside of the head coil. A post-experiment interview was conducted, during which we also asked participants to estimate what percentage of time they spent imagining future/remembering past episodes, or engaging in less-specific mind-wandering during the resting scan.

fMRI Image Acquisition

Participants were scanned with a 3T Siemens MRI scanner at Baycrest's Rotman Research Institute. A high-resolution 3D MPRAGE T1-weighted pulse sequence image (160 axial slices, 1 mm thick, FOV = 256 mm) was first obtained to register functional maps against brain anatomy. Functional imaging was performed to measure brain activation by means of the blood oxygenation level-dependent (BOLD) effect. Functional T2*-weighted images were acquired using echo-planar imagine (30 axial slices, 3.5 mm thick, TR = 2000 ms, TE = 24 ms, flip angle = 70 degrees, FOV = 20 cm2). The native EPI resolution was 64x64 with a voxel size of 3.5mm x 3.5mm x 3.5mm, with a 0.5 mm gap. Images were acquired using an oblique orientation (30 degree clockwise to the anterior–posterior commissure axis) to correct for signal dropout observed in the ventral medial prefrontal cortex. All subsequent analysis steps were conducted using the statistical parametric mapping software SPM8 [27]. Preprocessing involved slice timing correction, spatial realignment, and co-registration with a resampled voxel size of 3 mm isotropic with no smoothing. As all of our analyses rely on covariance, we additionally regressed out the mean time-courses from participant-specific white matter, and cerebrospinal fluid masks, alongside estimates of the 6 rigid body motion parameters from each EPI run. Again, to further correct for the effects of motion may persist despite standard processing [38] an identical additional motion scrubbing procedure was added to the end of our preprocessing pipeline [39]. Using a conservative multivariate technique, time points that were outliers in both the six rigid-body motion parameter estimates and BOLD signal were removed, where the BOLD signal was interpolated across using neighboring data points. Motion scrubbing further minimizes any effects of motion-induced spikes on the BOLD signal, over and beyond standard motion regression, without leaving sharp discontinuities due to the removal of outlier volumes (for details, see [39]).

QUANTIFICATION AND STATISTICAL ANALYSIS

fMRI Analysis: Inter-Voxel Similarity and Temporal Autocorrelation

FSL [28] (fslmeants) was used to extract separate voxelwise time courses per participant, per hippocampal mask, per EPI (i.e., a run of navigation). These hippocampal voxelwise time courses consisted of estimates of brain activity per TR per voxel from each participant-specific hippocampal mask, and were the basis of all subsequent analyses. All subsequent analyses were conducted using R and RStudio v.1.0.136 [30, 31]. Voxelwise activity estimates were z-scored per voxel, run, and participant. This ensured that each voxel's time course of activity was mean centered and on the same scale. To determine the neural similarity in activity across all voxels in the head and tail of the hippocampus, which we will refer to as inter-voxel similarity, we calculated the Pearson correlations between each pair of voxels in each of our four masks (i.e., head and tail, per hemisphere), generating four similarity matrices per participant. Inter-voxel similarity captures the correlation in activity across separate voxels in an ROI, thus providing a summary statistic reflecting the similarity in signal from spatially separable voxels in an ROI. This procedure is identical to standard approaches of calculating functional connectivity during resting fMRI, but here it is employed at the voxel level within an anatomical mask rather than the more common ROI-ROI approach. Average estimates of similarity were derived from each of these matrices by first applying a Fisher-Z transform to entire matrix, and removing the diagonal and upper triangle [32], leaving only one estimate of similarity between every pairwise combination of voxels, which were then averaged to produce an overall estimate of inter-voxel similarity. Averaged estimates of inter-voxel similarity were calculated per head/tail, hemisphere, and participant. These estimates were then submitted to a repeated-measures ANOVA with axis, hemisphere, and condition as factors. The individual correlation plots presented in the manuscript were created using [33].

Another measure of similarity was also calculated to better capture the temporal autocorrelation present in the hippocampus. This measure is independent from the initial measure of inter-voxel similarity, which captures the degree to which each voxel's time course correlates with the time course of every other voxel in the mask. Temporal autocorrelation instead reflects the average similarity within each voxel from time 1 to time 2. Admittedly, the temporal resolution available to fMRI is quite poor relative to electrophysiological measures in animals (e.g., maximum sampling rate of 0.5 HZ in present study, relative to high frequency electrophysiological recordings). However, the prevalence of this kind of measure in the rodent literature warranted the use of a conceptually similar measure in fMRI which would be sensitive to temporal autocorrelations despite being at a much coarser scale. Temporal autocorrelation was determined by calculating the Pearson correlation between the activity for each voxel within each hippocampal mask at TR 1 with the same set of voxels' activity at TR 2. This produced n - 1 estimates of similarity, where n is equal to the number of TRs per functional run, each representing how correlated all of the voxels were with themselves from time 1 to time 2 (i.e., temporal autocorrelation). These estimates were averaged per functional run, producing a single measure of autocorrelation per head/tail, hemisphere, functional run corresponding to a specific navigational condition, and participant. These estimates were then submitted to a repeated-measures ANOVA with the same factors as described above.

Temporal Autocorrelation across different Temporal Separations

To investigate the evolution of the autocorrelation signal over multiple time points rather than exclusively looking at one temporal separation (i.e., lag), we additionally calculated temporal autocorrelation for each of the 6 segments across 4 temporal separations (1 TR, 2 TRs, 3 TRs, and 4 TRs). For example, for the 1 TR separation, TR1 would be correlated with TR2 and TR2 with TR3; for the 2 TR separation, TR1 would be correlated with TR3, TR2 with TR4, etc. The results of this analysis are presented in Figures S2D and S2E.

To better illustrate the data, we extracted mean autocorrelation values per temporal separation for each of the axial segments. To be able to directly compare these values, we then standardized the autocorrelation values within each condition for each temporal separation. We then calculated the mean standardized autocorrelation across the four temporal separations for each of the navigation conditions and during rest (Figures S2F and S2G).

Native Space Masks

Native space hippocampal and parahippocampal cortex masks were extracted using FreeSurfer [17]. Hippocampal masks were then split into anterior and posterior segments manually, by using the position of the uncal apex as a conventional anatomical landmark [2]. Parahippocampal masks were split into anterior and posterior segments at the middle volume along their anterior-posterior extent.

To further probe the degree of similarity between voxels along the hippocampal anteroposterior axis irrespective of specific anatomical landmarks, we divided the hippocampal masks into smaller segments. We divided each participant's bilateral hippocampal masks into 6 segments along the anteroposterior axis. The location of the uncal apex, used to split the hippocampus into anterior and posterior portions, relative to these segments, is overlaid on an example participant's parcellation in Figure 4 in the main manuscript. We then again calculated inter-voxel similarity in the navigation and resting state experiments (see Figures S2 and S3).

Accounting for Hippocampal Shape in 2- and 6-Segment Parcellations

To exclude the possibility that the shape of the hippocampus contributed to our estimates of inter-voxel similarity and temporal autocorrelation, we accounted for the average distance between voxels in the x-, y-, and z-directions (see Figure S3). For example, the voxels in aHPC are closer to one another than voxels in pHPC, as pHPC is more elongated in the anteroposterior direction (Table S1). This average difference in distance between voxels may influence the similarity between voxel time courses within aHPC and pHPC ROIs. To exclude this as a possibility, we calculated the distance between individual voxels in the x-, y-, and z-directions, for both the 2 and 6-segment analyses, and included them in the existing model. Specifically, we took the x-, y- and z- coordinates for each voxel in a ROI, then calculated the absolute deviation between each voxel coordinate and the mean coordinate across all voxels, per direction, for each subject-specific mask. These deviations were then averaged per ROI, producing an estimate of the average distance (or, deviation in voxels) from the midpoint for the x-, y- and z- directions. We ran linear mixed effects models (R package 'nlme' [36]) predicting inter-voxel similarity and temporal autocorrelation from axis and hemisphere, with x-, y-, and z-distance values as covariates (akin to an ANCOVA).

Control Region of Interest: Parahippocampal Cortex

We sought to determine whether our findings were unique to the hippocampus, as would be suggested by the literature on place cells [9–11], or whether they captured a more general anteroposterior organizing principle of the brain not restricted to the hippocampus. An ideal control region would be a proximal extrahippocampal region that is highly connected to the hippocampus, providing a conservative test of whether the observed anteroposterior differences extend to a highly-connected neighboring region. We identified the parahippocampal cortex (PHC) as a control region corresponding to these criteria, as it is frequently involved in spatial processing [40, 41] and is highly coupled with the hippocampus [20]. Critically, the common long-axis orientation between the hippocampus and PHC (Figure S4) made the latter an ideal control to test whether general signal properties along the anteroposterior axis of the brain might account for the results presented here. Therefore, we divided participant-specific PHC masks into anterior and posterior portions (at the midpoint along the y axis), per hemisphere, and calculated inter-voxel similarity and temporal autocorrelation analyses on both the navigation and resting state datasets.

We directly compared aHPC and pHPC to anterior and posterior PHC (aPHC, pPHC) using 2 (region: HPC, PHC) x 2 (axis: anterior, posterior) x 2 (hemisphere: left, right) repeated-measures ANOVAs on measures of inter-voxel similarity and temporal autocorrelation.

Task Analysis

To examine whether hippocampal dynamics were modulated by task demands, we conducted additional mixed ANOVAs comparing the effects of hemisphere (left, right; within-subject), axis (anterior, posterior; within-subject), and task (navigation, rest; between-subject) on intervoxel similarity and temporal autocorrelation (Figure S4).

Spatial and Temporal Signal-to-Noise Ratio along the Hippocampal Axis

Spatial SNR was derived from participant-specific structural volumes, where the mean signal intensity for each hippocampal ROI was divided by the voxel-wise standard deviation from signal observed in a manually-placed control ROI outside of the brain (Table S2). The control ROI was a sphere with a 9 voxel radius (i.e., # of voxels = 3071, 1 mm isotropic voxels), and was positioned per participant such that it was non-overlapping with the head or any ringing artifact, permitting an appropriate estimation of the extraneous

variability present in our structural images. To address the possibility that greater spatial SNR in the pHPC contributed to our functional results, we ran two linear mixed effects where we added SNR as covariates to axis and hemisphere, predicting inter-voxel similarity and temporal autocorrelation.

Temporal SNR was calculated using AFNI (3dTstat -cvarinvNOD), which defines SNR as the mean of each voxel's time course divided by its standard deviation. SNR was calculated for left and right anterior and posterior hippocampal voxels and averaged per participant within each ROI using this approach (Table S3). For the navigation data, SNR was additionally averaged across conditions, as no condition-specific effects were expected. We first entered temporal SNR as the dependent variable in a linear mixed effects model with axis (aHPC, pHPC) and hemisphere (L, R) as factors. We next ran two linear mixed effects where we added SNR as covariates to axis and hemisphere, predicting inter-voxel similarity and temporal autocorrelation (mirroring the ANCOVA-like analysis applied to account for hippocampal shape; Figure S3).

DATA AND SOFTWARE AVAILABILITY

The code to run the analysis is available on GitHub (https://github.com/ivabrunec/Voxel_Temporal_Patterns). The fMRI data from the experiment is available upon request.